



Original Paper

Research on multi-wave joint elastic modulus inversion based on improved quantum particle swarm optimization

Peng-Qi Wang^a, Xing-Ye Liu^{b,*}, Qing-Chun Li^{a,**}, Yi-Fan Feng^a, Tao Yang^a,
Xia-Wan Zhou^a, Xu-Kun He^a

^a College of Geological Engineering and Geomatics, Chang'an University, Xi'an, 710054, Shaanxi, China

^b State Key Laboratory of Geohazard Prevention and Geoenvironment Protection, College of Geophysics, Chengdu University of Technology, Chengdu, 610059, Sichuan, China



ARTICLE INFO

Article history:

Received 19 April 2024

Received in revised form

19 July 2024

Accepted 21 October 2024

Available online 22 October 2024

Edited by Meng-Jiao Zhou

Keywords:

Young's modulus

PP-PS joint inversion

Exact Zoeppritz

Pre-stack inversion

QPSO

ABSTRACT

Young's modulus and Poisson's ratio are crucial parameters for reservoir characterization and rock brittleness evaluation. Conventional methods often rely on indirect computation or approximations of the Zoeppritz equations to estimate Young's modulus, which can introduce cumulative errors and reduce the accuracy of inversion results. To address these issues, this paper introduces the analytical solution of the Zoeppritz equation into the inversion process. The equation is re-derived and expressed in terms of Young's modulus, Poisson's ratio, and density. Within the Bayesian framework, we construct an objective function for the joint inversion of PP and PS waves. Traditional gradient-based algorithms often suffer from low precision and the computational complexity. In this study, we address limitations of conventional approaches related to low precision and complicated code by using Circle chaotic mapping, Lévy flights, and Gaussian mutation to optimize the quantum particle swarm optimization (QPSO), named improved quantum particle swarm optimization (IQPSO). The IQPSO demonstrates superior global optimization capabilities. We test the proposed inversion method with both synthetic and field data. The test results demonstrate the proposed method's feasibility and effectiveness, indicating an improvement in inversion accuracy over traditional methods.

© 2024 The Authors. Publishing services by Elsevier B.V. on behalf of KeAi Communications Co. Ltd. This is an open access article under the CC BY license (<http://creativecommons.org/licenses/by/4.0/>).

1. Introduction

In recent years, challenges associated with conventional reservoirs have driven increased interest in exploring and producing from unconventional resources (Zhou et al., 2021; Wang et al., 2022; Chen et al., 2022a). Specifically, investigating shale reservoirs often necessitates hydraulic fracturing (Ding et al., 2022). Rock physics research highlights Young's modulus and Poisson's ratio as crucial indicators for evaluating rock brittleness and fracture intensity (Yin and Zhang, 2014; Song et al., 2023). Therefore, accurately extracting parameters related to Young's modulus and Poisson's ratio from seismic data is crucial for comprehensive reservoir characterization, brittleness assessment, and predicting optimal drilling zones in unconventional oil and gas fields (Wang et al., 2022; Zhou et al., 2022a).

Pre-stack seismic data contain extensive geological, lithological, fluid, and other relevant information (Buland and Omre, 2003; Yan et al., 2021). The amplitude versus offset (AVO) technique is essential for extracting elastic parameters from pre-stack seismic datasets. Significant advances in AVO inversion technology have made it a widely used tool in the modern petroleum industry (Ahmed et al., 2023; Chen et al., 2022b; Ouyang et al., 2023). AVO analysis relies heavily on evaluating the reflection coefficient between subsurface media, as described by the Zoeppritz equation (Pan et al., 2019). Due to its complexity, the Zoeppritz equation has been approximated under various idealized conditions by scholars (Aki and Richards, 1980; Shuey, 1985; Smith and Gidlow, 1987; Fatti et al., 1994). Substantial research based on these approximate equations has produced widely adopted industry findings. However, the derivation of the approximate reflection coefficient formula requires assumptions of small incident angles and weak parameter contrasts, which may limit the effective handling of seismic amplitude information, especially at far offsets (Wang et al., 2023). Furthermore, these approximation conditions result in the

* Corresponding author.

** Corresponding author.

E-mail addresses: lxylxx@cdu.edu.cn (X.-Y. Liu), dclqic@chd.edu.cn (Q.-C. Li).

formula being relatively insensitive to changes in density, thereby reducing the accuracy of provided density information. Consequently, despite its simplified form, the approximated equation inherently restricts the accuracy of pre-stack inversion (Zhi et al., 2018; Cheng et al., 2022). Therefore, pre-stack inversion based on the exact Zoeppritz equation is a critical step towards enhancing inversion accuracy.

Brittleness is a critical factor in unconventional oil and gas exploration. The key parameters for predicting sweet spots and assessing brittleness are Young's modulus and Poisson's ratio (Zhou et al., 2017). Typically, reservoirs with high Young's modulus and lower Poisson's ratio exhibit increased brittleness. These parameters are also essential for calculating the reservoir's brittleness index, providing valuable guidance for horizontal well placement and hydraulic fracturing strategies (Li et al., 2021; Miao et al., 2024). Young's modulus and Poisson's ratio are generally determined through indirect methods. The indirect method involves obtaining velocity and density information from seismic data, followed by the calculation of Young's modulus and Poisson's ratio using petrophysical relations. However, this indirect approach is susceptible to cumulative errors, which can reduce the accuracy of the inversion process.

In response to the limitations of indirect inversion methods, numerous scholars have developed direct inversion approaches for determining Young's modulus and Poisson's ratio. These approaches involve deriving reflection coefficient equations that explicitly include Young's modulus and Poisson's ratio. Zong et al. (2012) derived a linear relationship between the PP wave reflection coefficient and Young's modulus, Poisson's ratio, and density (YPD equation) from the Aki approximate equation. The reflection coefficient formula, derived from the approximate equation, is susceptible to assumptions of small incident angles and weak parameter contrasts, leading to inaccurate inversion results. Adopting the exact Zoeppritz equation can partially address these issues. Chen et al. (2022a) transformed the PP wave equation from the exact Zoeppritz equation into a form that includes Young's modulus, Poisson's ratio, and density, proposing a nonlinear inversion approach with promising application results in practical fields. Similarly, Song et al. (2023) conducted a comparable derivation and applied it to sandstone reservoirs. These studies aim to further derive the exact Zoeppritz equation into a new form that incorporates Young's modulus, Poisson's ratio, and density for application in subsequent inversion studies.

The inversion of PP waves using the exact Zoeppritz equation has been extensively researched by numerous scholars, yielding significant findings. However, seismic inversion problems are often ill-posed, making it difficult to obtain reliable estimates from PP wave seismic data alone (Liu and Xia, 2004; Yang and Wang, 2022). In contrast, PS wave seismic data contain abundant information about density and fluid properties (Damasceno et al., 2021). Integrating PS wave seismic records into the PP-PS wave joint inversion process can produce more accurate inversion results, reduce uncertainty in reservoir interpretation, and improve inversion accuracy. Lavaud et al. (1999) used the adjoint state method for joint PP-PS nonlinear inversion and showed that the addition of PS AVO information improves the inversion results. Russell et al. (2005) used the PP-PS wave joint inversion to invert for acoustic impedance and density. Khare and Rape (2007) examined the sensitivity of joint inversion of PP/PS data to different PP and PS angle ranges.

The joint inversion of PP-PS waves, based on the exact Zoeppritz equation, represents a highly nonlinear problem (Grechka et al., 1999; Jenkinson et al., 2010; Lu et al., 2015). Traditional gradient-based algorithms lack the accuracy required to handle such complexity (Liu et al., 2023a, 2023b). Swarm intelligence optimization algorithms, which are based on meta-heuristics,

demonstrate excellent global optimization performance, versatility, and suitability for parallel processing, making them valuable tools for solving geophysical inverse problems (Liu et al., 2024; Pan et al., 2017; Tang et al., 2023). Many scholars have investigated the application of intelligent optimization algorithms in geophysics (Grana et al., 2022; Meng et al., 2023; Shi et al., 2024). Particle swarm optimization (PSO), a conventional intelligent optimization algorithm, has been widely applied in the engineering (Kennedy and Eberhart, 1995). However, issues pertaining to its limited global optimization performance and the intricacies associated with parameter settings have become increasingly pronounced. The quantum particle swarm optimization (QPSO) algorithm, which incorporates quantum behavior, eliminates dependence on the directional movement attribute of particles (Sun et al., 2004, 2012). This modification makes the update of particle positions independent of their previous movements, thereby enhancing their positional randomness and significantly improving global optimization capabilities. It is noteworthy that the quantum particle swarm optimization (QPSO) also has the flaw of easily falling into local minima, and scholars have conducted extensive research on improvements to intelligent optimization algorithms. Improvements to intelligent optimization algorithms typically involve increasing the initial population diversity and incorporating mutation strategies, among other methods. Building on previous enhancements, this paper introduces Circle chaotic mapping to mitigate issues like clustering of initial solutions, inadequate coverage in the solution space, and limited diversity among individuals, thereby enhancing sample diversity. Studies have shown that incorporating the Lévy flight strategy into intelligent optimization algorithms can help avoid local minima and improve global search optimization capabilities. In pre-stack AVO inversion, the inversion results for density are inferior to other parameters. This is mainly due to the insensitivity of density in the inversion objective function. To address this issue, this paper introduces a Gaussian mutation strategy specifically into the density term inversion to improve the inversion accuracy of the density term. Integrating these improvement strategies, we propose an enhanced quantum particle swarm optimization named improved quantum particle swarm optimization (IQPSO).

We present a precise solution form of the exact Zoeppritz equation, which is subsequently rederived to include only Young's modulus, Poisson's ratio, and density. Within the Bayesian inversion framework, we then construct a nonlinear inversion objective function. To solve this objective function, the newly introduced IQPSO algorithm is employed. The efficacy of the proposed method was evaluated using both single well synthetic and actual production data. Test results indicate that our proposed Young's modulus nonlinear inversion method, based on the exact Zoeppritz equation, accurately extracts Young's modulus and Poisson's ratio from seismic data. This research offers a novel method for reservoir prediction and formation brittleness evaluation.

2. Methodology

2.1. Derivation of the reflection coefficient formula expressed in terms of Young's modulus, Poisson's ratio, and density

The primary objective of AVO inversion is to extract P-wave velocity, S-wave velocity, and density from pre-stack seismic data. Commonly, traditional inversion methods rely on the approximate reflection coefficient formulas. To achieve greater accuracy in the inversion process, this study adopts the exact Zoeppritz equation as the forward operator. The exact Zoeppritz equation describes the relationships among elastic parameters, reflection coefficients, and transmission coefficients when P waves are incident on the

interface of isotropic media, as detailed in Eq. (1).

$$\begin{bmatrix} \sin \theta_1 & \cos \varphi_1 & -\sin \theta_2 & \cos \varphi_2 \\ -\cos \theta_1 & \sin \varphi_1 & -\cos \theta_2 & -\sin \varphi_2 \\ \sin 2\theta_1 & \frac{V_{P1}}{V_{S1}} \cos 2\varphi_1 & \frac{\rho_2 V_{S2}^2 V_{P1}}{\rho_1 V_{S1}^2 V_{P2}} \sin 2\theta_2 & \frac{-\rho_2 V_{S2} V_{P1}}{\rho_1 V_{S1}^2} \cos 2\varphi_2 \\ \cos 2\varphi_1 & \frac{-V_{S1}}{V_{P1}} \sin 2\varphi_1 & \frac{-\rho_2 V_{P2}}{\rho_1 V_{P1}} \cos 2\varphi_2 & \frac{-\rho_2 V_{S2}}{\rho_1 V_{P1}} \sin 2\varphi_2 \end{bmatrix} \begin{bmatrix} R_{PP} \\ R_{PS} \\ T_{PP} \\ T_{PS} \end{bmatrix} = \begin{bmatrix} -\sin \theta_1 \\ -\cos \theta_1 \\ \sin 2\theta_1 \\ -\cos 2\varphi_1 \end{bmatrix} \quad (1)$$

In the above formula, R_{PP} , R_{PS} , T_{PP} and T_{PS} represent the PP wave reflection coefficient, PS wave reflection coefficient, PP wave transmission coefficient and PS wave transmission coefficient, respectively. V_P represents the P wave velocity, V_S represents the PS wave velocity, ρ represents the density, and the subscripts 1 and 2 respectively represent the medium parameters on the upper and lower sides of the interface. Furthermore, θ and φ represent the angles of the PP wave and the PS wave respectively, and the subscripts 1 and 2 represent the reflection angle and transmission angle respectively.

As shown in Eq. (1), the exact form of the Zoeppritz equation is notably intricate. During program implementation, frequent inversion operations are necessary, which may compromise solution accuracy. To address this challenge, Aki and Richards (1980) solved the exact Zoeppritz equation and provided a more concise solution form. The formulations in Eqs. (2) and (3) articulate the exact solutions for the reflection coefficients of PP waves and PS waves. This paper primarily focuses on the analytical solutions for the PP wave reflection coefficient and PS reflection coefficient in its discussions.

$$R_{PP} = \frac{E^- F - G^+ H P^2}{D} \quad (2)$$

$$R_{PS} = -2 \frac{\cos \theta_1}{V_{P1}} \left(ab + cd \frac{\cos \theta_2}{V_{P2}} \frac{\cos \varphi_2}{V_{S2}} \right) P V_{P1} / (V_{S1} D) \quad (3)$$

where,

$$\begin{cases} a = \rho_2 (1 - 2V_{S2}^2 P^2) - \rho_1 (1 - 2V_{S1}^2 P^2) \\ b = \rho_2 (1 - 2V_{S2}^2 P^2) + 2\rho_1 V_{S1}^2 P^2 \\ c = \rho_1 (1 - 2V_{S1}^2 P^2) + 2\rho_2 V_{S2}^2 P^2 \\ d = 2\rho_2 V_{S2}^2 - 2\rho_1 V_{S1}^2 \\ E^+ = b \frac{\cos \theta_1}{V_{P1}} + c \frac{\cos \theta_2}{V_{P2}} \\ E^- = b \frac{\cos \theta_1}{V_{P1}} - c \frac{\cos \theta_2}{V_{P2}} \\ F = b \frac{\cos \varphi_1}{V_{S1}} + c \frac{\cos \varphi_2}{V_{S2}} \\ G^+ = a + d \frac{\cos \theta_1}{V_{P1}} \frac{\cos \varphi_2}{V_{S2}} \\ G^- = a - d \frac{\cos \varphi_1}{V_{P1}} \frac{\cos \varphi_2}{V_{S2}} \\ H = a - d \frac{\cos \theta_2}{V_{P2}} \frac{\cos \varphi_1}{V_{S1}} \\ D = E^+ F + G^- H P^2 \end{cases}$$

The parameter P in the above formula is given by Snell's law:

$$P = \frac{\sin \theta_1}{V_{P1}} = \frac{\sin \theta_2}{V_{P2}} = \frac{\sin \varphi_1}{V_{S1}} = \frac{\sin \varphi_2}{V_{S2}} \quad (4)$$

The relationship between Young's modulus, P wave velocity, and S wave velocity can be expressed as Eq. (5):

$$\begin{cases} E_1 = \frac{3V_{P1}^2 - 4V_{S1}^2}{V_{P1}^2 - V_{S1}^2} \cdot \rho_1 V_{S1}^2 \\ E_2 = \frac{3V_{P2}^2 - 4V_{S2}^2}{V_{P2}^2 - V_{S2}^2} \cdot \rho_2 V_{S2}^2 \end{cases} \quad (5)$$

Poisson's ratio is the absolute value of the ratio of transverse strain to longitudinal strain, effectively reflecting the rock's physical properties and the fluid information of the reservoir. Its relationship with the velocities is expressed in Eq. (6):

$$\begin{cases} \left(\frac{V_{P1}}{V_{S1}} \right)^2 = \frac{2(1 - \sigma_1)}{1 - 2\sigma_1} \\ \left(\frac{V_{P2}}{V_{S2}} \right)^2 = \frac{2(1 - \sigma_2)}{1 - 2\sigma_2} \end{cases} \quad (6)$$

Substituting Eqs. (4)–(6) into Eqs. (2) and (3), the reflection

coefficient equation represented by Young's modulus, Poisson's ratio, and density can be obtained:

$$R_{pp} = \left(\tilde{e} - \tilde{f} - \frac{2N_1\rho_1\tilde{g}^+\tilde{h}\sin^2\theta}{M_1E_1} \right) / \tilde{D} \quad (7)$$

$$R_{PS} = -2 \cos \theta \sqrt{\frac{2N_1\rho_1}{M_1E_1}} \left(\tilde{a}\tilde{b} + \tilde{c}\tilde{d} \sqrt{\frac{2N_2\rho_2}{M_2E_2} - \frac{2N_1\rho_1 \sin^2 \theta}{M_1E_1}} \right) \sqrt{\frac{2N_2\rho_2}{E_2} - \frac{2N_1\rho_1 \sin^2 \theta}{M_1E_1}} \sin \theta / \left(\tilde{D}^* \sqrt{\frac{E_1}{2N_1\rho_1}} \right) \quad (8)$$

where,

$$\begin{aligned} \tilde{a} &= \rho_2 \left(1 - \frac{2E_2N_1\rho_1 \sin^2 \theta}{E_1M_1N_2\rho_2} \right) - \rho_1 \left(1 - \frac{2 \sin^2 \theta}{M_1} \right) \tilde{b} \\ &= \rho_2 \left(1 - \frac{2E_2N_1\rho_1 \sin^2 \theta}{E_1M_1N_2\rho_2} \right) + \rho_1 \frac{2 \sin^2 \theta}{M_1}, \\ \tilde{c} &= \frac{2E_2N_1\rho_1 \sin^2 \theta}{E_1M_1N_2} + \rho_1 \left(1 - \frac{2 \sin^2 \theta}{M_1} \right), \tilde{d} = \frac{E_2}{N_2} - \frac{E_1}{N_1}, \tilde{e} \\ &= \tilde{b} \cdot \cos \theta \cdot \sqrt{\frac{2N_1\rho_1}{M_1E_1}} + \tilde{c} \cdot \sqrt{\frac{2N_2\rho_2}{M_2E_2} - \frac{2N_1\rho_1 \sin^2 \theta}{M_1E_1}}, \\ \tilde{e}^- &= \tilde{b} \cdot \cos \theta \cdot \sqrt{\frac{2N_1\rho_1}{M_1E_1}} - \tilde{c} \cdot \sqrt{\frac{2N_2\rho_2}{M_2E_2} - \frac{2N_1\rho_1 \sin^2 \theta}{M_1E_1}}, \tilde{f} \\ &= \tilde{b} \sqrt{\frac{2N_1\rho_1}{E_1} - \frac{2N_1\rho_1 \sin^2 \theta}{M_1E_1}} + \tilde{c} \cdot \sqrt{\frac{2N_2\rho_2}{E_2} - \frac{2N_1\rho_1 \sin^2 \theta}{M_1E_1}}, \\ \tilde{g} &= \tilde{a} - \tilde{d} \cdot \cos \theta \sqrt{\frac{4N_1N_2\rho_1\rho_2}{M_1E_1E_2} - \frac{4N_1^2\rho_1^2 \sin^2 \theta}{M_1^2E_1^2}}, \tilde{g}^+ \\ &= \tilde{a} + \tilde{d} \cdot \cos \theta \sqrt{\frac{4N_1N_2\rho_1\rho_2}{M_1E_1E_2} - \frac{4N_1^2\rho_1^2 \sin^2 \theta}{M_1^2E_1^2}}, \\ \tilde{h} &= \tilde{a} - \tilde{d} \sqrt{\frac{2N_2\rho_2}{M_2E_2} - \frac{2N_1\rho_1 \sin^2 \theta}{M_1E_1}} \cdot \sqrt{\frac{2N_1\rho_1}{E_1} - \frac{2N_1\rho_1 \sin^2 \theta}{M_1E_1}}, \tilde{D} \\ &= \tilde{e}\tilde{f} + \frac{2\tilde{g}\tilde{h}N_1\rho_1 \sin^2 \theta}{M_1E_1} \end{aligned}$$

$$N_1 = 1 + \sigma_1, N_2 = 1 + \sigma_2, M_1 = \frac{2(1 - \sigma_1)}{1 - 2\sigma_1}, M_2 = \frac{2(1 - \sigma_2)}{1 - 2\sigma_2}$$

To evaluate the accuracy of the rewritten R_{pp} equation based on the analytical solution of the Zoeppritz equation, we selected the gas-bearing sandstone and shale model proposed by Ostrander

Table 1
Model for gas-bearing sandstone and shale.

	V_p , km/s	V_s , km/s	Den, g/cm ³	E , 10 ⁹ N/m ²	σ
Model I	3.048	1.244	2.4	10.3999	0.4001
	2.438	1.625	2.14	12.4354	0.1003
Model II	2.438	1.625	2.14	12.4354	0.1003
	3.048	1.244	2.4	10.3999	0.4001

(1984). We compared the rewritten reflection coefficient equation, the Aki-Richards approximation formula, and the exact Zoeppritz equation. The model data are shown in Table 1, and the comparison results are shown in Fig. 1.

2.2. Construction of inversion objective function

Most geophysical inverse problems are characterized as ill-posed (Liu et al., 2023b; Zhou et al., 2022b). Within the Bayesian framework, inversion serves a dual purpose: it not only aims to identify an optimal solution but also facilitates uncertainty analysis of the inversion outcomes within a probabilistic paradigm (Pan et al., 2019). A key distinction from classical statistical theory is the incorporation of prior information. Consequently, formulating an objective function under the Bayesian framework to derive the maximum posterior probability distribution of a numerical model is widely regarded as a robust and effective approach for tackling geophysical inverse problems.

$$P(\mathbf{m}|\mathbf{d}) = \frac{P(\mathbf{d}|\mathbf{m})P(\mathbf{m})}{P(\mathbf{d})} \propto P(\mathbf{d}|\mathbf{m})P(\mathbf{m}) \quad (9)$$

Among them, \mathbf{d} is the actual observation record, \mathbf{m} is the model parameter. $P(\mathbf{m})$ is the prior probability of the model, that is, the model parameters are constrained through some experience, such as previous research data, geological information, drilling data, Stratigraphic sections, etc. $P(\mathbf{d}|\mathbf{m})$ is the probability of the observation data \mathbf{d} under the condition of the model \mathbf{m} , which is called the likelihood function. $P(\mathbf{d})$ is the marginal probability distribution of the observation data \mathbf{d} . $P(\mathbf{m}|\mathbf{d})$ is the posterior probability of model \mathbf{m} under the condition of observation record \mathbf{d} .

The outcomes of probabilistic Bayesian inversion methods often exhibit significant uncertainties. To address this, the prior distribution of model parameters is incorporated to enhance constraints and improve the well-posedness of the inversion. Commonly used prior distributions encompass the Gaussian, Huber, and Cauchy distributions. Each distribution imparts distinct general characteristics, leading to varying regularization constraints. Assuming that the model parameters (Young's modulus, Poisson's ratio, and density) follow the three-variable modified Cauchy distribution, then:

$$P(\mathbf{m}) = \frac{1}{\pi^{(2n_d)}|\boldsymbol{\chi}|^{n_d/2}} \exp\left(-\sum_{i=1}^{n_d} \frac{(\mathbf{m} - \boldsymbol{\omega})^T \boldsymbol{\zeta}_i (\mathbf{m} - \boldsymbol{\omega})}{1 + (\mathbf{m} - \boldsymbol{\omega})^T \boldsymbol{\zeta}_i (\mathbf{m} - \boldsymbol{\omega})}\right) \quad (10)$$

Among them, $\boldsymbol{\chi}$ is a 3×3 covariance matrix containing the statistical correlation between model parameters, $\boldsymbol{\omega}$ is the average value of the model parameters, obtained from prior information. $\boldsymbol{\zeta}_i = \mathbf{D}_i^T \boldsymbol{\chi}^{-1} \mathbf{D}_i$, where \mathbf{D}_i is a 3×3 n_d matrix, and its specific form is:

$$[\mathbf{D}_i]_{xy} = \begin{cases} 1 & \text{if } x = 1 \text{ and } y = i \\ 1 & \text{if } x = 2 \text{ and } y = i + n_d \\ 1 & \text{if } x = 3 \text{ and } y = i + 2n_d \\ 0 & \text{else} \end{cases} \quad (11)$$

The construction of the likelihood function typically relies on a noise model. A common assumption in this context is that the noise follows a Gaussian distribution, leading to the formulation of the likelihood function as:

$$P(\mathbf{d}|\mathbf{m}) = \frac{1}{\sqrt{(2\pi)^{n_d} |C_d|}} \exp\left(-\frac{1}{2}(\mathbf{d} - \mathbf{G}(\mathbf{m}))^T C_d^{-1} (\mathbf{d} - \mathbf{G}(\mathbf{m}))\right) \quad (12)$$

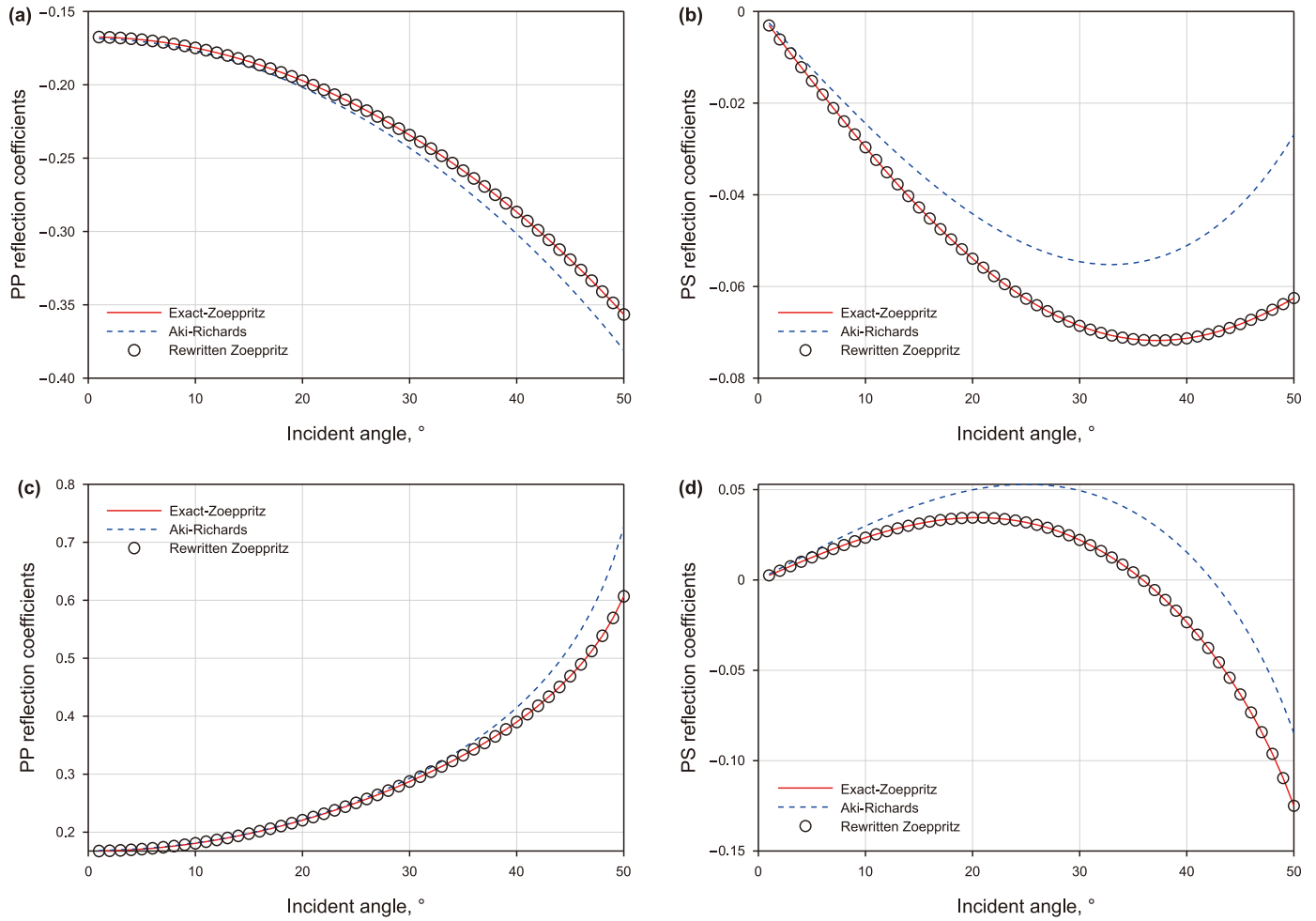


Fig. 1. Comparison of different reflection coefficient formulas. (a)–(b) Model I; (c)–(d) Model II.

where, C_d represents the covariance matrix of data noise, and $G(\mathbf{m})$ is the theoretical data obtained by forward modeling of model \mathbf{m} . According to the prior probability and likelihood function of the model parameters, the posterior probability of the model parameters can be obtained to satisfy:

which is the constraint item for a prior information. $\mu = \sigma_{n_d}^2$, represents the variance of the data noise, serving as a weight factor to regulate the influence of prior information in the weighting process.

PP-PS joint inversion reduces the uncertainty of the inversion by

$$P(\mathbf{m}|\mathbf{d}) \propto \exp\left(-\frac{1}{2}(\mathbf{d} - \mathbf{G}(\mathbf{m}))^T C_d^{-1} (\mathbf{d} - \mathbf{G}(\mathbf{m})) - \sum_{i=1}^{n_d} \frac{(\mathbf{m} - \omega)^T \zeta_i (\mathbf{m} - \omega)}{1 + (\mathbf{m} - \omega)^T \zeta_i (\mathbf{m} - \omega)}\right) \quad (13)$$

Applying the natural logarithm to both sides of Eq. (13) and multiplying the result by -1 to convert the maximum value of the posterior distribution probability function into the minimum value of the following objective function:

$$J(\mathbf{m}) = \frac{1}{2}(\mathbf{d} - \mathbf{G}(\mathbf{m}))^T (\mathbf{d} - \mathbf{G}(\mathbf{m})) + \mu \Gamma(\mathbf{m}) \quad (14)$$

where,

$$\Gamma(\mathbf{m}) = \sum_{i=1}^{n_d} \frac{(\mathbf{m} - \omega)^T \zeta_i (\mathbf{m} - \omega)}{1 + (\mathbf{m} - \omega)^T \zeta_i (\mathbf{m} - \omega)},$$

introducing S wave seismic data. Extending Eq. (14) to multi-wave seismic data, the objective function of joint longitudinal and transverse wave inversion number can be obtained, as shown in Eq. (15), where τ is the weight coefficient that controls the participation of PS wave data in the inversion. The value of τ is determined by the ratio of the noise variances of the PP and PS waves. Let the noise variance of the PP wave seismic data be σ_{pp} , and the noise variance of the PS wave seismic data be σ_{ps} , then $\tau = \sigma_{pp}/\sigma_{ps}$. In actual seismic records, the weight of PS-waves is obtained through multiple tests of seismic data near the well, typically, a value of 1 can be used for testing.

$$J(\mathbf{m}) = \frac{1}{2}(\mathbf{d}_{PP} - \mathbf{G}_{PP}(\mathbf{m}))^T(\mathbf{d}_{PP} - \mathbf{G}_{PP}(\mathbf{m})) + \frac{\tau}{2}(\mathbf{d}_{PS} - \mathbf{G}_{PS}(\mathbf{m}))^T(\mathbf{d}_{PS} - \mathbf{G}_{PS}(\mathbf{m})) + \mu\Gamma(\mathbf{m}) \quad (15)$$

2.3. Improved quantum particle swarm optimization

Inspired by the regularity of birds' foraging behavior, Kennedy and Eberhart (1995) proposed the traditional particle swarm optimization (PSO) algorithm. The PSO algorithm is characterized by its simplicity, ease of implementation, and fast convergence speed. However, it also suffers from several drawbacks, including the need to set numerous parameters, poor global optimization capabilities, and tendency to fall into local minima. Sun et al. (2004, 2012) introduced the concept of qubits to make particles have quantum behavior and proposed a quantum particle swarm optimization algorithm (QPSO). In the QPSO algorithm, each particle's position is represented as a probability distribution rather than a fixed value, which enhances the global search ability and allows for greater exploration in the search space. Building on previous work, this study further optimizes and improves the QPSO by multiple enhancement strategies. By employing multiple strategies to enhance the QPSO algorithm, we introduced an improved Quantum Particle swarm optimization, which we have named IQPSO.

The core of the QPSO algorithm lies in transforming the deterministic description of particles' positions and velocities into a probabilistic description, a change achieved by simulating the behavior of quantum particles. Quantum particles differ from classical particles in that they do not follow a definite trajectory, and their positions are expressed as probability density functions. In the QPSO algorithm, particles lack velocity vectors, so during the i_{th} iteration, the particle update can be described as:

$$\begin{aligned} X_{(i+1)} &= P_i - \beta*(mBest - X_i)*\ln(1/u) & k \geq 0.5 \\ X_{(i+1)} &= P_i + \beta*(mBest - X_i)*\ln(1/u) & k < 0.5 \end{aligned} \quad (16)$$

where,

$$P_i = \varphi*pBest_i + (1 - \varphi)*gBest_i \quad (17)$$

$$mBest = \frac{1}{N} \sum_{i=1}^N pBest_i \quad (18)$$

$mBest$ represents the average best position of the particle population, defined as the average of all particles' best positions (global optimal position). $pBest$ denotes the best position of a particle during the current iteration (individual optimal position). N represents the number of particles in the population. In the QPSO algorithm, P_i serves as a local attraction factor, determined by both the individual optimal position and the global optimal position. The φ in the expression is a random number between 0 and 1. In Eq. (16), both k and u are random numbers between 0 and 1.

Parameter β , the only manually specified constant in the QPSO algorithm, is termed the compression-expansion coefficient, which regulates the algorithm's convergence speed. β plays a critical role in the algorithm; a larger β value facilitates global exploration in the early stages, while a smaller β is suitable for local optimization in the later stages. In this paper, we set β to linearly decrease within the range between 0.5 and 1 according to Eq. (19), i denotes the current iteration count, Nl indicates the total number of iterations.

$$\beta = \frac{(\beta_{max} - \beta_{min})*(i - 1)}{Nl} + \beta_{min} \quad (19)$$

The above process describes the particle updating process in the QPSO algorithm. Compared to the PSO algorithm, the QPSO algorithm features simpler parameter design and stronger global optimization capabilities; however, it still tends to fall into local minima. In intelligent optimization algorithms, the quality of optimization results largely depends on the initial population's exploration of the solution space. The classical QPSO algorithm initializes the population using functions that generate a normal distribution. Populations generated by this method lack randomness and uniformity, failing to effectively cover the entire solution space. To address this issue, we implemented Circle chaotic mapping for population initialization, as described in Eq. (20).

$$x_{i+1} = \text{mod} \left(x_i + 0.2 - \left(\frac{0.5}{2\pi} \right) \sin(2\pi x_i), 1 \right) \quad (20)$$

Fig. 2 illustrates the results of population distributions generated by two distinct functions for a population size of 200. The initialization method using chaotic mapping shows a more orderly overall population distribution compared to the random initialization method. The random initialization assumes that the population follows a normal distribution with a mean of 0.5, resulting in a concentration around the this mean. In contrast, the chaotic mapping initialization provides a more structured distribution, offering greater exploration possibilities for particles, ensuring population diversity, and reducing the risk of convergence to local optima (Verma et al., 2022). Therefore, introducing Circle chaotic mapping for population initialization allows for a more thorough exploration of the solution space, enhancing the algorithm's global optimization capabilities. Another approach to prevent QPSO algorithms from getting trapped in local minima is the introduction of the Lévy flight strategy. The Lévy flight strategy involves a random walk after each iteration, jumping to positions relatively far from the current optimum and recalculating the fitness values. If the fitness value at this new position is lower than that at the current optimum, it is considered an escape from the local minimum. The formula for this random walk is expressed as:

$$x_{i+1} = x_i + \alpha*\text{sign}[\text{rand} - 1/2] \oplus \text{Levy}(\mu) \quad (21)$$

The step length of Lévy flight is $\text{Levy}(\mu)$, which can be expressed as

$$\text{Levy}(\mu) = \frac{\mu}{|v|^{1/\beta}} \quad (22)$$

where, β is defined as one constant. In our work, we let $\beta = 1.5$, $\mu = N(0, \sigma_\mu^2)$, and v is a random number between 0 and 1.

Regardless of the improvement strategy employed, the multiple solutions and ill-posed of geophysical inverse problems must be considered. Particularly in AVO inversion, the density parameter is relatively insensitive to the inversion objective function. A Gaussian mutation strategy has been introduced for the density term. By implementing a Gaussian mutation strategy, normally distributed random numbers are applied at probability p to the current optimal position to create new positions. In this paper, a high mutation probability is set, with p valued at 0.6. The purpose of introducing the Gaussian mutation strategy is to increase the variety of search possibilities for the density term and enhance the algorithm's sensitivity to this parameter. The mutation process is described as follows:

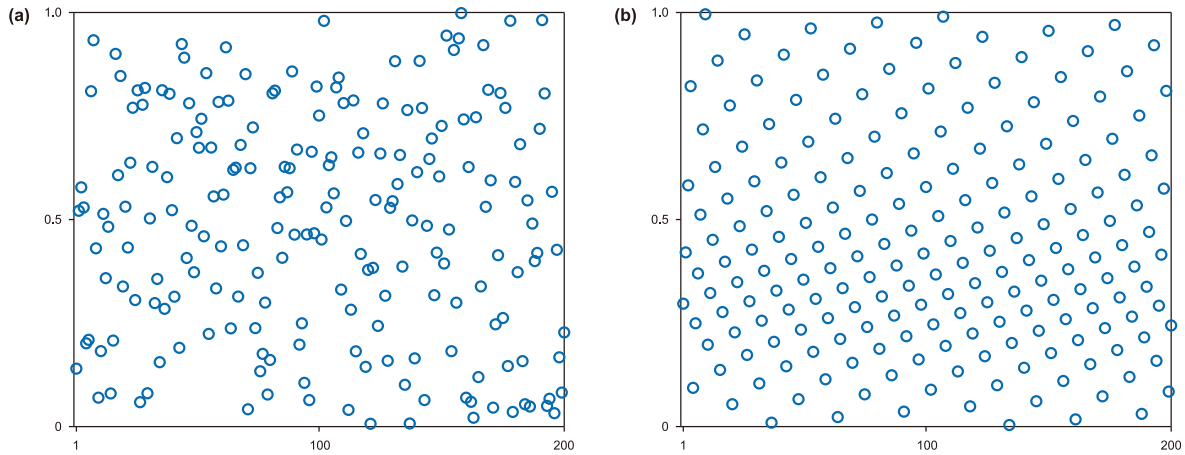


Fig. 2. Distribution of the initial populations of different methods. (a) Rand; (b) circle chaotic mapping.

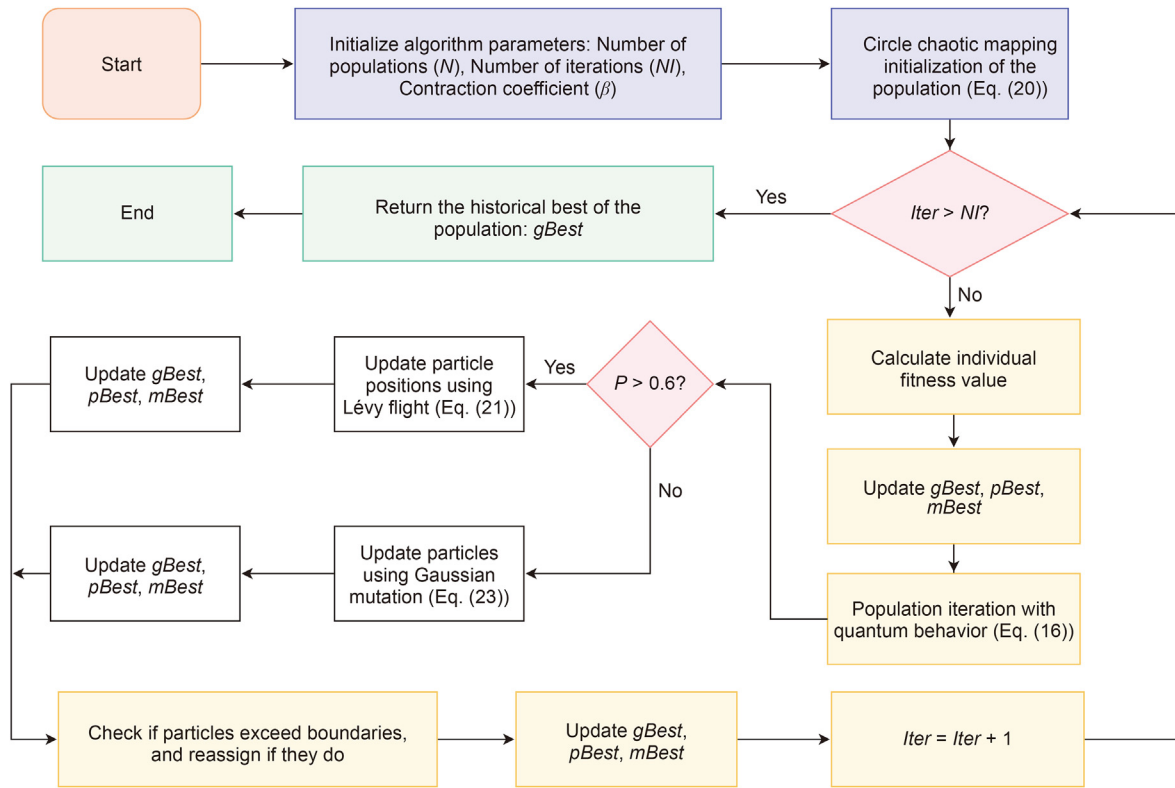


Fig. 3. The flowchart of IQPSO.

$$x_{best}(i + 1) = x_{best}(i) * (1 + \text{Gaussan}(\sigma)) \quad (23)$$

$$\text{Gaussan}(\sigma) = \frac{1}{\sqrt{2\pi}\sigma} e^{-\frac{(x-\mu)^2}{2\sigma^2}} \quad (24)$$

The introduction of the Circle chaotic mapping strategy has improved the initial population's exploration of the solution space, aiding in a thorough search by the algorithm. By incorporating the Lévy flight strategy, the algorithm's global optimization capacity is strengthened, avoiding the pitfalls of local minima. Furthermore, by specifically introducing a Gaussian mutation strategy, the algorithm becomes more sensitive to the density term in geophysical inversion problems, enhancing the precision of density inversion.

With these three strategic improvements, the newly proposed IQPSO algorithm is more suitable for the inversion problems discussed in this paper, with further enhanced global search capabilities. Comparative tests with examples are provided later. The flowchart of the IQPSO algorithm is shown in Fig. 3.

3. Synthetic seismic recording test

In this section, synthetic angle gather seismic records are used to evaluate the inversion effect and reliability of the proposed Young's modulus nonlinear inversion method based on the exact Zoeppritz equation. Using real well data, Young's modulus and Poisson's ratio curves are constructed as model parameters to be

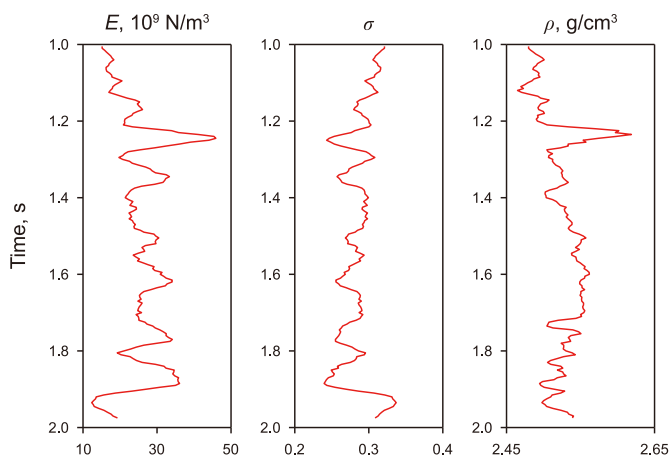


Fig. 4. Model parameters to be estimated. E is the Young's modulus data; σ is the Poisson's ratio; ρ is the density.

estimated, as shown in Fig. 4.

The range of incidence angles for the synthetic multi-wave seismic data from 1° to 45° . The PP and PS wave reflection coefficients at different incidence angles are calculated using the newly accurate reflection coefficient form, as shown in Eqs. (7) and (8). Convolution of the obtained reflection coefficients with a Ricker wavelet, which has a dominant frequency of 30 Hz, generates the synthetic multi-wave seismic recordings. To assess the noise resistance of the proposed algorithm, Gaussian random noise with signal-to-noise ratios (SNR) of 2 and 5 is added to the noiseless synthetic seismic records, producing noisy synthetic seismic records, as shown in Fig. 5. It is particularly important to note that, when the signal-to-noise ratio is 2, $\sigma_{PP}/\sigma_{PS} = 0.9216$, when the signal-to-noise ratio is 5, $\sigma_{PP}/\sigma_{PS} = 0.9458$.

Intelligent optimization algorithms require predefined parameter ranges when addressing geophysical inverse problems. To simulate the conditions of actual seismic inversion, this paper sets a hard constraint for the iteration range to fluctuate up and down 30% from the real value. Additionally, the conventional least squares iterative algorithm for comparison to evaluate the nonlinear inversion effects of Young's modulus based on the exact Zoeppritz equation. To better demonstrate the advantages of the method proposed in this paper, the following comparisons of different inversion methods were conducted. Fig. 6 shows the

inversion results under different noise conditions using the nonlinear inversion method proposed in this paper. Fig. 7 shows the inversion results obtained indirectly through the Aki-Richards formula. Fig. 8 shows the results of direct joint PP-PS wave inversion using the least squares algorithm. In Figs. 6–8, the blue lines represent the inversion results, and the red lines represent the true values of the model. To compare the inversion results of different methods more intuitively, Fig. 9 presents the mean relative errors (MRE) of Young's modulus, Poisson's ratio, and density under different inversion methods and noise conditions.

The comparison in Fig. 6(a)–(c) demonstrates that the inversion method introduced can reliably and efficiently estimate Young's modulus, Poisson's ratio, and density values from seismic data. Although the inversion accuracy decreases with increasing noise, reasonable estimations of the approximate model values remain achievable. Comparing Figs. 6 and 7, the inversion accuracy in Fig. 7, based on the approximate formula for indirect inversion, is lower than that of Fig. 6, especially between 1.8 s and 2.0 s. Comparing our proposed method with conventional iterative algorithms for joint PP-PS inversion, as shown in Figs. 6 and 8, reveals that although the accuracy of iterative algorithms in noise-free environments closely aligns with this study's method, they fall short in terms of density inversion accuracy. We attribute the improved density inversion precision to the incorporation of random Gaussian variations into the density parameter. Under noisy conditions, the inversion performance of the method introduced is significantly superior to that of iterative algorithms, as supported by the data on average relative errors. Thus, test results from single well data indicate that the inversion accuracy for Young's modulus, Poisson's ratio, and density, using the method proposed in this study with a new exact solution derived from the precise Zoeppritz equation, exceeds traditional methods, yielding superior results.

To evaluate the superiority of the IQPSO algorithm proposed in this study, we conducted tests using noise-free synthetic seismic data as an example. Fig. 10(a) presents the fitness value curves for different algorithms as the number of iterations increases. Fig. 10(b) displays the fitness values across different iteration counts, given the same size for the initial population. The x-axis represents the number of iterations, and the y-axis denotes the fitness value. Fig. 10(c) compares the inversion results using the PSO algorithm and IQPSO algorithm on noise-free synthetic seismic records. Fig. 10(a) reveals that the IQPSO algorithm secured the lowest fitness values, with a noticeable stepwise reduction in fitness. It is important to note that the parameters set for computation using

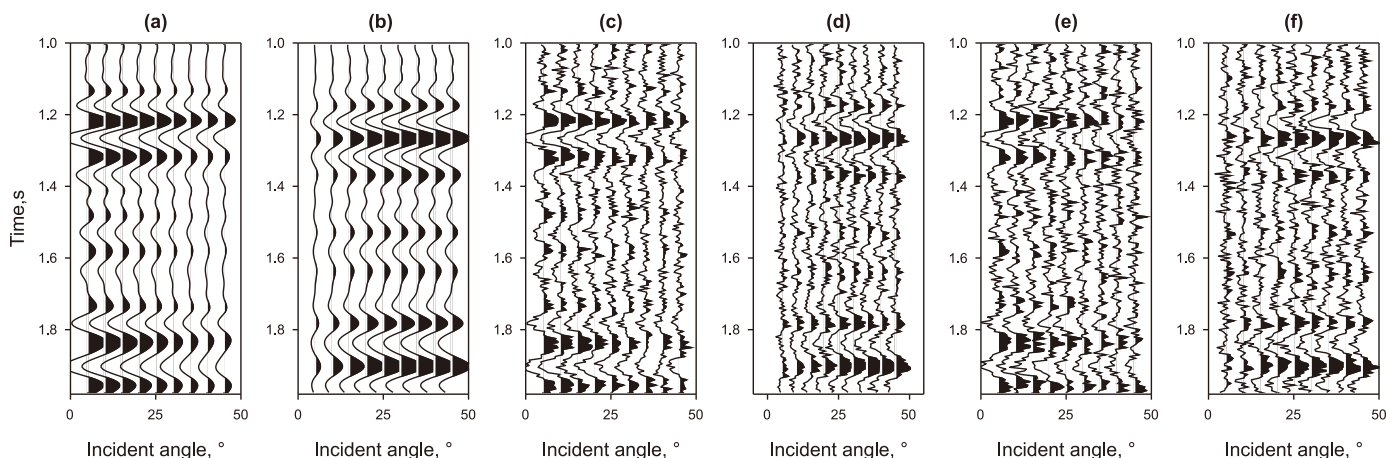


Fig. 5. Synthetic prestack angle gathers. (a)–(b) PP and PS wave angles gather without noise; (c)–(d) PP and PS wave angles gather with added random noise with noise S/N = 5; and (e)–(f) PP and PS wave angles gather with added random noise with noise S/N = 2.

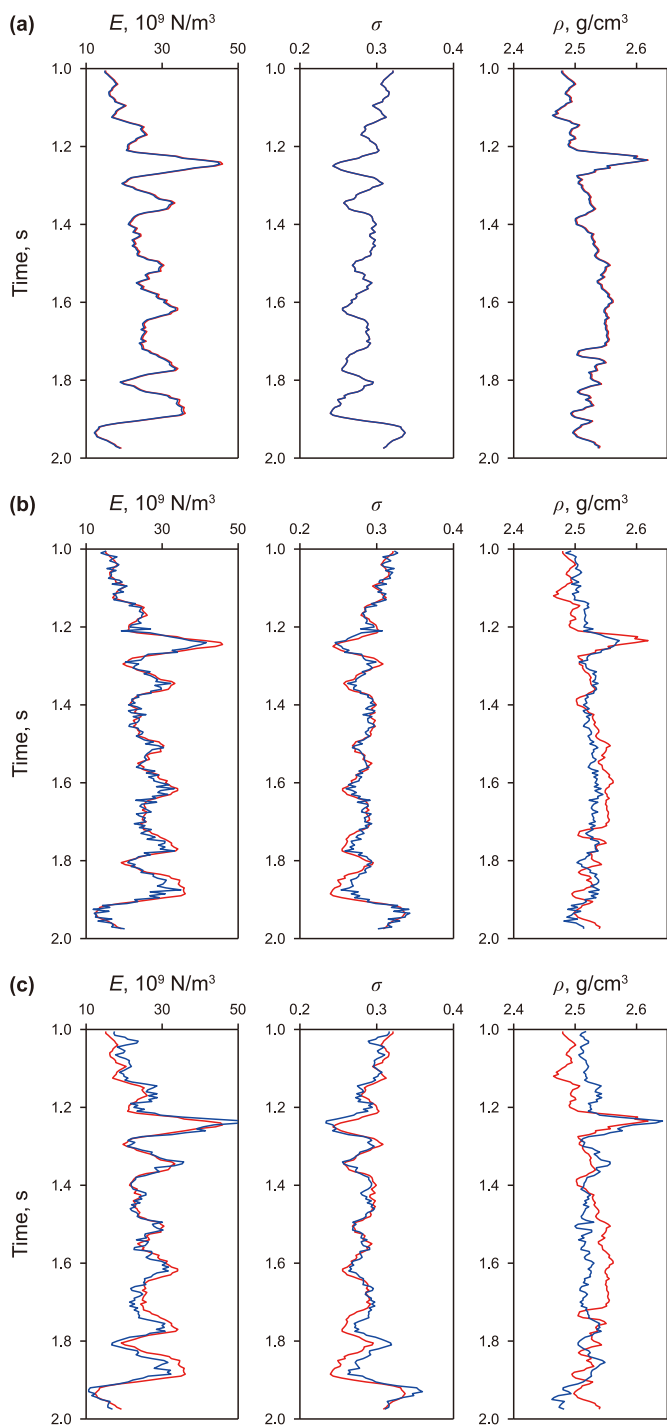


Fig. 6. Inversion results (the proposed method, PP and PS joint direct inversion). Blue line indicates inversion result and red line indicates true model data. E is the Young's modulus data; σ is the Poisson's ratio; ρ is the density. (a) Noise free; (b) $S/N = 5$; (c) $S/N = 2$.

the PSO and IQPSO algorithms are identical, with the iteration count (NI) set to 800. The population size is set to 200, and the iteration range is defined as $\pm 30\%$ of the true value. In the PSO algorithm, the self-learning factor (c_1) is set to 2, the social learning factor (c_2) is set to 2, and the inertia weight adaptively changes from 0.9 to 0.4, the adaptive change formula is $\omega = \omega_{\max} - [(\omega_{\max} - \omega_{\min}) \cdot \text{iter}] / NI$, where iter represents the current number of iterations, and NI is the total number of iterations. This

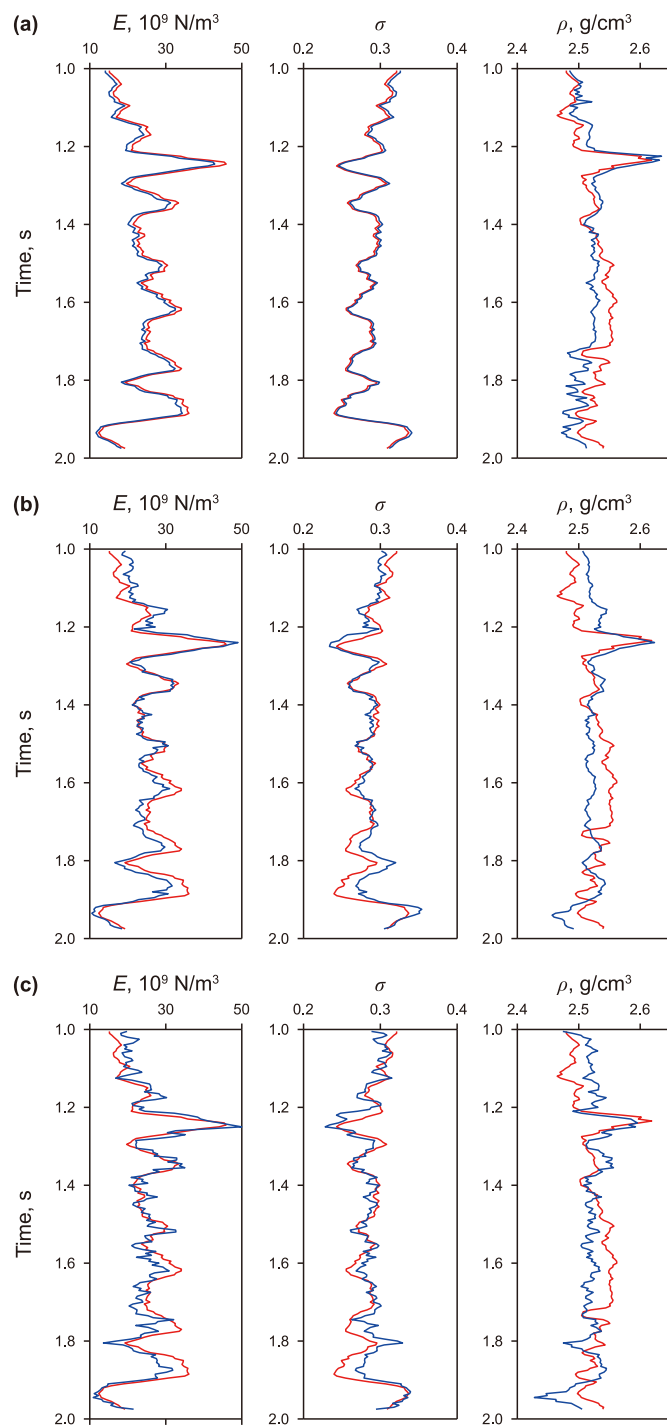


Fig. 7. Inversion results (PP wave inversion based on the approximate formula, indirect inversion). Blue line indicates inversion result and red line indicates true model data. E is the Young's modulus data; σ is the Poisson's ratio; ρ is the density. (a) Noise free; (b) $S/N = 5$; (c) $S/N = 2$.

commendable performance is attributed to the incorporation of Gaussian mutations into the density term, which lowered the fitness value and improved inversion precision. Analyzing Fig. 10(b) reveals that while the IQPSO algorithm initially underperformed compared to the QPSO algorithm, it successfully escaped local minima and achieved global optimization as the iteration count increased.

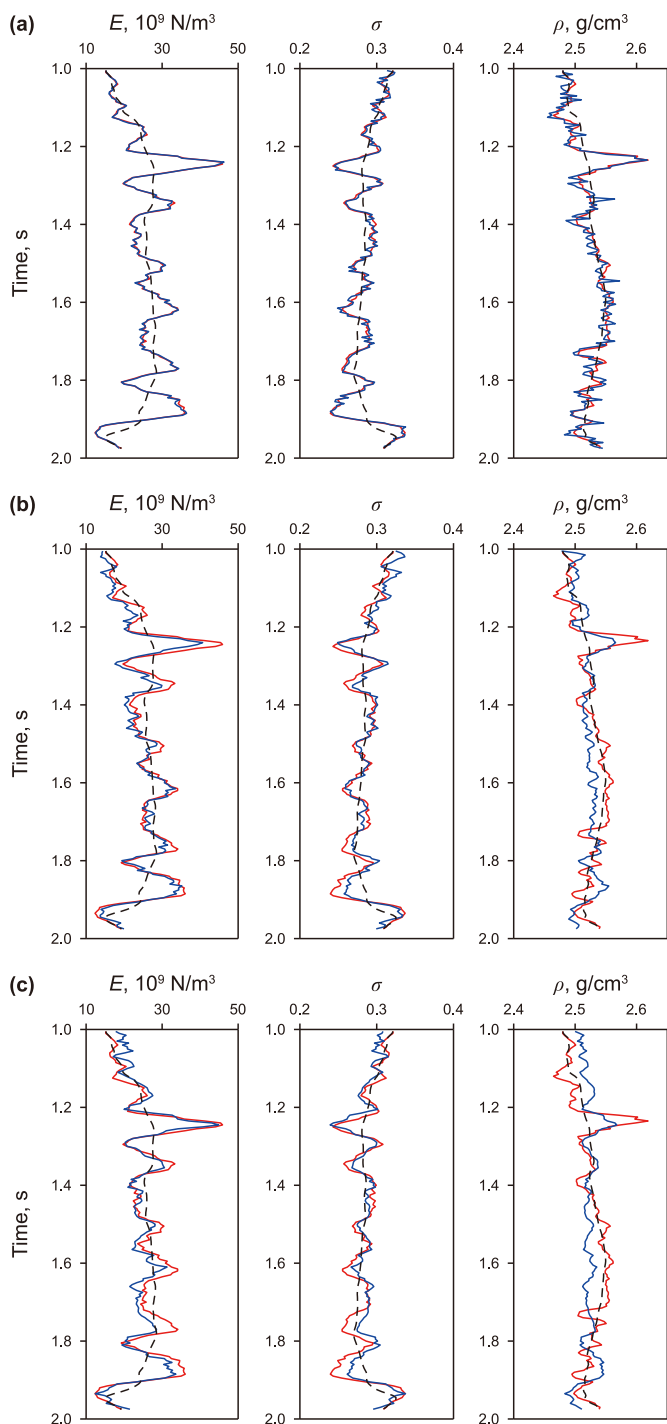


Fig. 8. Inversion results (PP and PS joint inversion by the linear direct inversion method). Blue line indicates inversion result and red line indicates true model data, the black dashed line represents the initial data. E is the Young's modulus data; σ is the Poisson's ratio; ρ is the density. (a) Noise free; (b) S/N = 5; (c) S/N = 2.

4. Testing with field data

To evaluate the application effectiveness of the PP-PS joint inversion method based on the new accurate solution form of the exact Zoppritz equation on field data, we excerpted some open seismic data for testing. The open data was sourced from the Volve oil field in the Norwegian North Sea, with the *Hugin* formation being the main reservoir of interest. The field data is available in the

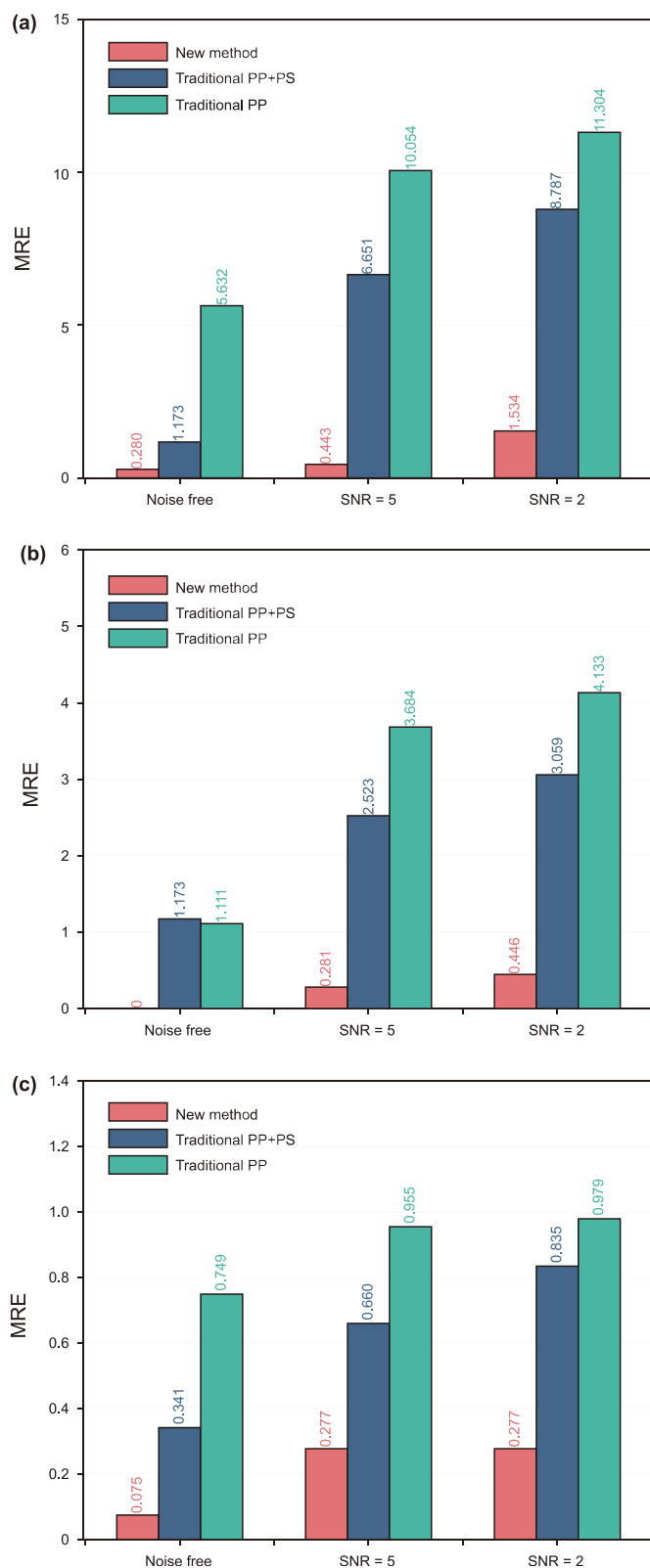


Fig. 9. Mean relative error. (a) The Young's modulus inversion results; (b) the Poisson's ratio inversion results; (c) the density inversion results.

Equinor dataset. The data was subjected to a range of standard processing steps, including amplitude compensation and adjustment, deconvolution, noise suppression, NMO correction,

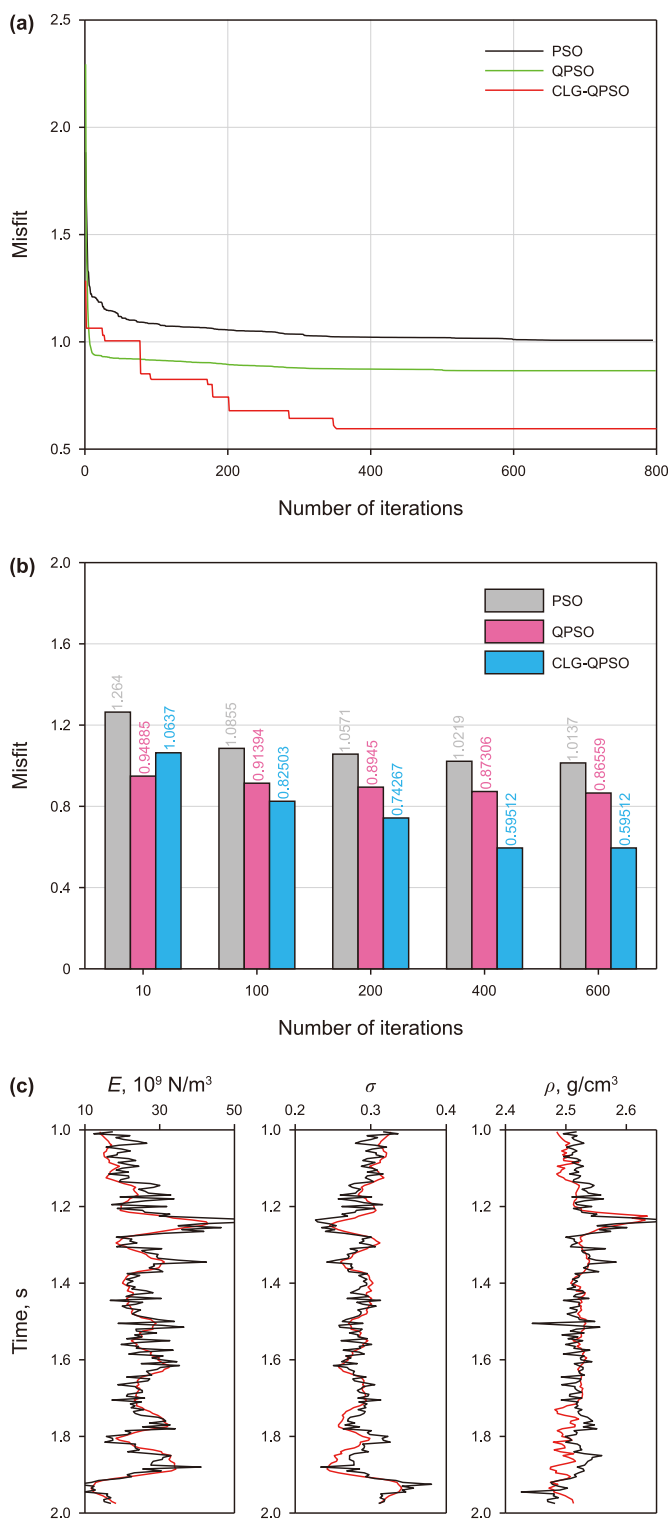


Fig. 10. Comparison of inversion efficiency of IQPSO and PSO, taking noise-free synthetic seismic data as an example. (a) Convergence curves of different algorithms; (b) fitness values of different algorithms; (c) black line is the inversion result by PSO, the red line is the inversion result by IQPSO.

suppression of interbed multiples, and pre-stack time migration. The pre-stack seismic data was time-matched, with PS wave seismic data represented in PP wave time. To conveniently test the reliability of the proposed method, we selected a portion of the field data for testing. Fig. 11(a) and (b) display the stack profiles of

the test area, with Fig. 11(a) representing the PP wave stack profile and Fig. 11(b) representing the PS wave stack profile. The black lines in the images mark the positions of well in the test area.

Angle stack data from the work area was extracted for testing at angles of 5°, 14°, 23°, 32°, and 41°, and phase seismic wavelet were extracted from the wells for inversion. Fig. 12 shows the inversion results for Young's modulus, Poisson's ratio, and density using the method proposed in this study. Fig. 13 shows the PP wave inversion results for Young's modulus, Poisson's ratio, and density data with traditional iterative algorithms. The black line in Fig. 13 represents the information of the filtered well log curve. To better demonstrate the inversion effect, Fig. 14 provides the inversion curves for the seismic traces at the well locations. The blue lines in Fig. 14 represent the well log values, and the red lines represent the inversion results using the method proposed in this paper. Comparing Figs. 12 and 13, the inversion results of the method proposed in this paper have a higher lateral resolution than those of iterative algorithms, offering clearer delineation of target layers and better inversion effects. According to the core sampling results disclosed in the Equinor dataset, the main target layer in the test area is the Hugin formation sandstone reservoir (2600 ms), and the inversion results clearly show the low-value anomaly of this layer.

Moreover, a comparison with well logs reveals that the inversion outcomes from the proposed method, despite exhibiting some discrepancies, generally align with the logging curve trends. This alignment provides interpreters with a reliable indication of the formation's Young's modulus and Poisson's ratio. Therefore, in practical field applications, this method can offer theoretical guidance for horizontal well placement and help identify approximate location of oil and gas reservoirs, thereby reducing exploration risks and increasing the success rate of drilling.

5. Discussion

Currently, Young's modulus is primarily obtained through approximate formula inversion or indirect calculation of elastic parameters, which often fails to meet the accuracy required for industrial applications. To address this issue, this paper proposes a pre-stack AVO inversion method based on the exact Zoeppritz equation to invert Young's modulus, Poisson's ratio, and density directly and simultaneously. Unlike other methods relying on approximate formulas, this approach re-derives exact solution of the Zoeppritz equation as the forward operator, effectively avoiding the impact of assumptions such as small incidence angles and low formation contrast inherent to approximate formulas, thereby enhancing inversion accuracy. Considering the complex form of the exact Zoeppritz equation, we have adopted the exact solution form of the Zoeppritz equation provided by Aki-Richards, which simplifies the forward operator while maintaining the same accuracy as the precise Zoeppritz equation. Additionally, this paper employs a PP-PS wave joint inversion strategy, which, by incorporating shear wave seismic information as opposed to traditional PP wave inversion, can reduce inversion uncertainty. This represents an advancement over the work of other scholars.

Considering the nonlinearity of the constructed inversion objective function, this paper introduces and improves the quantum particle swarm optimization, proposing a hybrid optimization quantum particle swarm optimization named IQPSO. The improved algorithm demonstrates significantly higher accuracy in inversion results for nonlinear seismic inversion problems compared to traditional gradient-based iterative algorithms. In nonlinear inversion algorithms, conventional nonlinear algorithms are highly dependent on the initial model and require extensive formula derivation for obtaining derivatives and Jacobian matrices. In contrast, intelligent optimization algorithms based on random

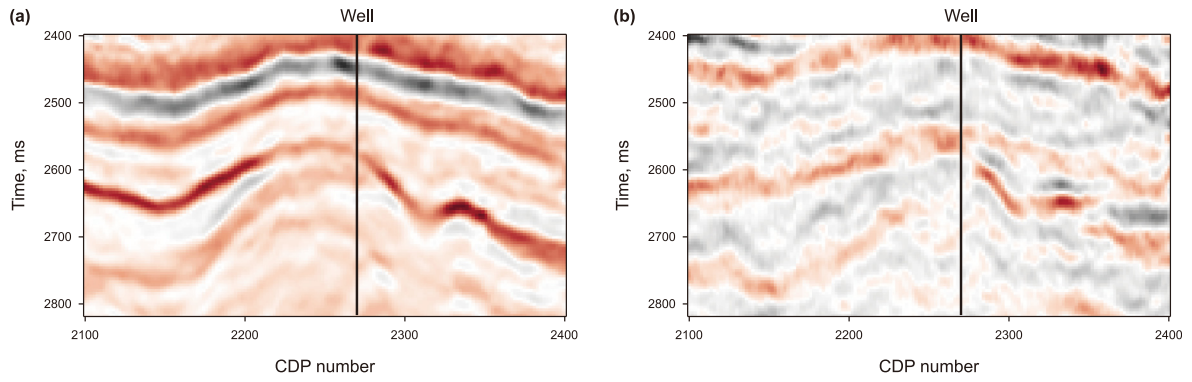


Fig. 11. Stack seismic profile. Black line indicates the location of well. (a) PP wave; (b) PS wave.

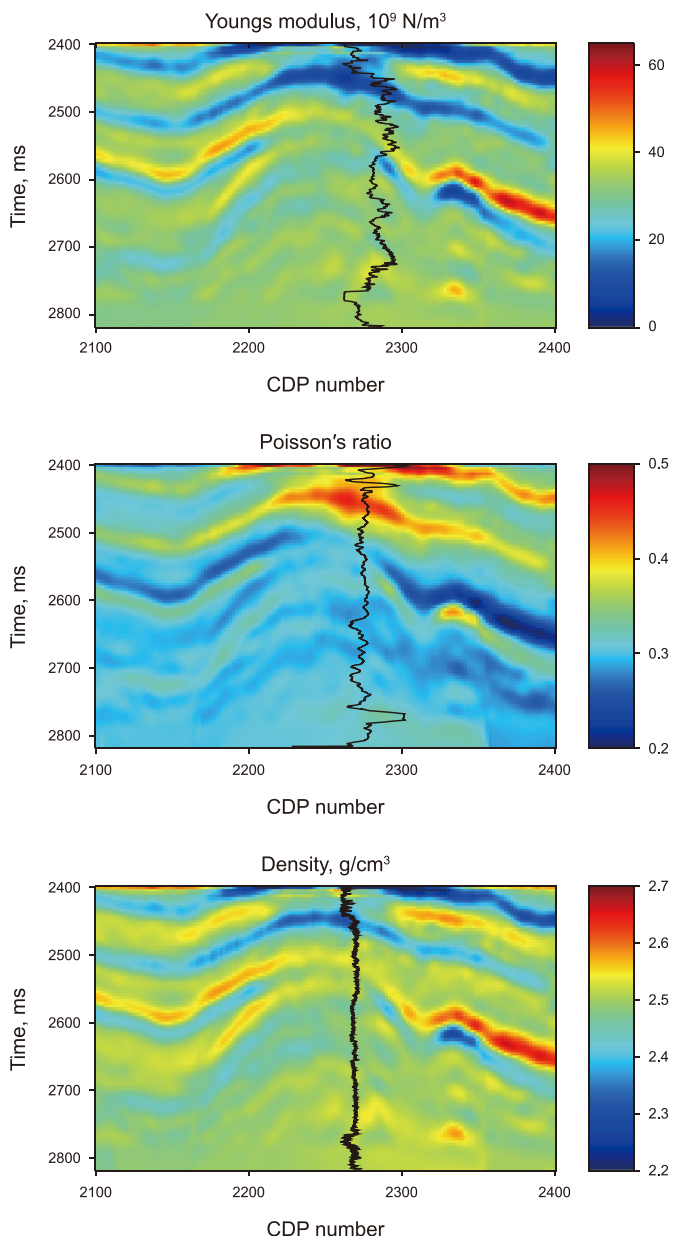


Fig. 12. Inversion results section of the proposed method. The black line is the well log curves after sparseness.

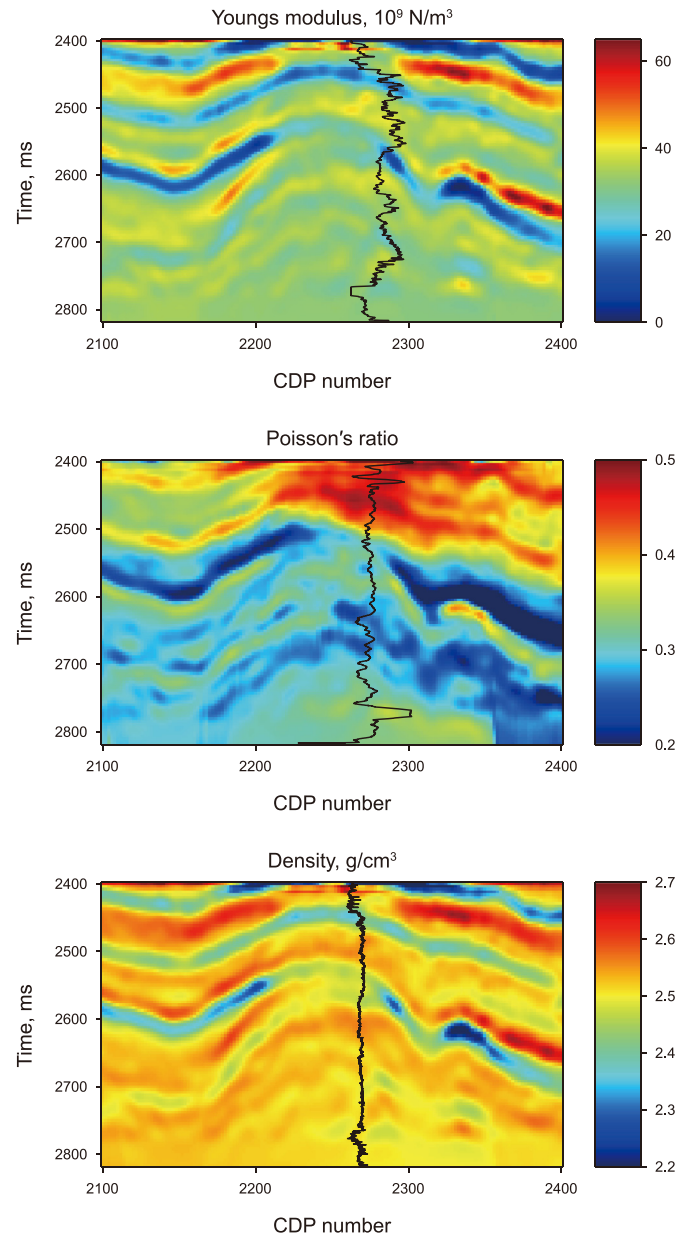


Fig. 13. PP wave inversion results section of the Aki-Richards approximation formula method. The black line is the well log curves after sparseness.

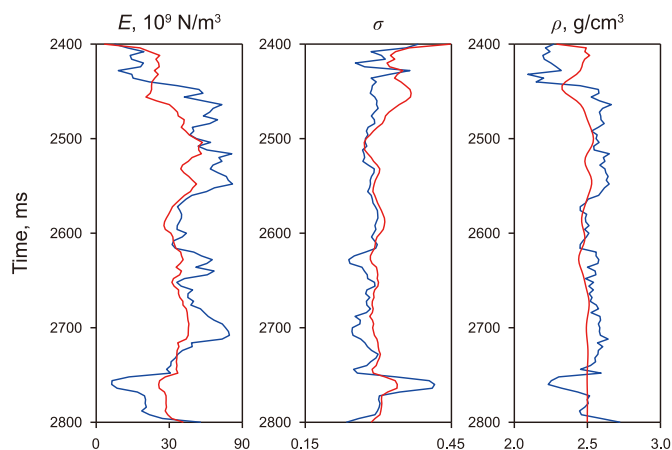


Fig. 14. Comparison of the well curve in the time domain and inverted result at the well location. Blue line indicates the well curves and red line indicates the inversion results of the proposed method. E is the Young's modulus data; σ is the Poisson's ratio; ρ is the density.

search only need a specified search range and are less dependent on the initial model. However, the drawback of these algorithms is that they require significant computational power and a substantial amount of time. Nonetheless, with the continuous improvement in computer processing capabilities, especially the enhancement of multicore parallel processing, this limitation should be mitigated. Notably, our method addresses cumulative errors from the indirect calculation of Young's modulus and Poisson's ratio, offering theoretical guidance for identifying sweet spots in shale reservoirs and deploying horizontal hydraulic fracturing wells.

6. Conclusion

Indirect inversion of Young's modulus introduces cumulative errors, reducing inversion accuracy. This paper introduces the exact solution form of the Zoeppritz equation and re-derives it in terms of Young's modulus, Poisson's ratio, and density. Within the Bayesian framework, we developed a joint PP-PS waves inversion process for Young's modulus, Poisson's ratio, and density. Additionally, this paper improves quantum particle swarm optimization algorithm for inversion. The inversion results of both synthetic data and actual data show that the method proposed in this paper is superior to the iterative algorithm in terms of inversion accuracy. Specifically, synthetic data illustrate that the targeted introduction of Gaussian mutation strategies in the inversion of density terms enhances the inversion effect of density items, confirming the feasibility and effectiveness of the method proposed in this paper.

Furthermore, in the discussion section, we also address the shortcomings of applying intelligent optimization algorithms, which are issues that need to be directly confronted in future research on such algorithms. In summary, the joint PP-PS wave inversion of Young's modulus, Poisson's ratio, and density based on the exact solution of the Zoeppritz equation, is both feasible and valuable for practical application.

CRediT authorship contribution statement

Peng-Qi Wang: Writing – original draft, Software, Project administration, Methodology, Investigation, Formal analysis, Data curation, Conceptualization. **Xing-Ye Liu:** Writing – review & editing, Supervision, Methodology. **Qing-Chun Li:** Writing – review & editing, Funding acquisition. **Yi-Fan Feng:** Validation, Investigation. **Tao Yang:** Investigation, Data curation. **Xia-Wan**

Zhou: Investigation. **Xu-Kun He:** Investigation.

Declaration of competing interest

The authors declare that they have no known competing financial interests or personal relationships that could have appeared to influence the work reported in this paper.

Acknowledgements

This work was supported by Fundamental Research Funds for the Central Universities, CHD300102264715, National Key Research and Development Program of China under Grant 2021YFA0716902, and Natural Science Basic Research Program of Shaanxi 2024JC-YBMS-199. We appreciate Equinor for providing the open-source seismic data. We gratefully acknowledge the helpful comments from the editors and anonymous reviewers, which greatly improved this manuscript.

References

- Ahmed, N., Weibull, W.W., Quintal, B., Grana, D., Bhakta, T., 2023. Frequency-dependent AVO inversion applied to physically based models for seismic attenuation. *Geophys. J. Int.* 233, 234–252. <https://doi.org/10.1093/gji/ggac461>.
- Aki, K., Richards, P.G., 1980. *Quantitative Seismology-Theory and Methods*. Mill Valley. University Science Books, California New York.
- Buland, A., Omre, H., 2003. Bayesian linearized AVO inversion. *Geophysics* 68 (1), 185–198. <https://doi.org/10.1190/1.1543206>.
- Chen, X., Zong, Z., Yang, Y., Zeng, Y., 2022a. Frequency-dependent nonlinear AVO Inversion for Q-factors in viscoelastic media. *IEEE Trans. Geosci. Rem. Sens.* 61, 1–17. <https://doi.org/10.1109/TGRS.2022.3233357>.
- Chen, X., Zong, Z., Zuo, Y., 2022b. Direct exact nonlinear broadband seismic amplitude variations with offset inversion for Young's modulus. *IEEE Trans. Geosci. Rem. Sens.* 61, 1–16. <https://doi.org/10.1109/TGRS.2022.3233594>.
- Cheng, J.W., Zhang, F., Li, X.Y., 2022. Nonlinear amplitude inversion using a hybrid quantum genetic algorithm and the exact Zoeppritz equation. *Petrol. Sci.* 19 (3), 1048–1064. <https://doi.org/10.1016/j.petsci.2021.12.014>.
- Damasceno, A., Tura, A., Simmons, J., 2021. The added value of joint PP-PS inversion for reservoir characterization: a case study using Jubarte PRM seismic data (offshore Brazil). *Geophys. Prospect.* 70 (1), 121–134. <https://doi.org/10.1111/1365-2478.13145>.
- Ding, J., Clark, A.C., Vanorio, T., Jew, A.D., Bargar, J.R., 2022. Elastic anisotropy of shales: the roles of crack alignment and compliance ratio. *Geophysics* 87 (2), A13–A17. <https://doi.org/10.1190/geo2021-0517.1>.
- Fatti, J.L., Smith, G.C., Vail, P.J., Strauss, P.J., Levitt, P.R., 1994. Detection of gas in sandstone reservoirs using AVO analysis: a 3-D seismic case history using the Geostack technique. *Geophysics* 59 (9), 1362–1376. <https://doi.org/10.1190/1.1443695>.
- Grana, D., Azevedo, L., de figueiredo, L., Connolly, P., Mukerji, T., 2022. Probabilistic inversion of seismic data for reservoir petrophysical characterization: review and examples. *Geophysics* 87 (5), M199–M216. <https://doi.org/10.1190/geo2021-0776.1>.
- Grechka, V., Theophanis, S., Tsvankin, I., 1999. Joint inversion of P- and PS-waves in orthorhombic media: theory and a physical modeling study. *Geophysics* 64 (1), 146–161. <https://doi.org/10.1190/1.1444512>.
- Jenkinson, T., Bansal, R., Martinez, A., Matheny, M., Khare, V., Cornaglia, V., 2010. Joint PP-PS angle-stack analysis and AVA inversion in Grane Field, offshore Norway. *Lead. Edge* 29 (10), 1228–1239. <https://doi.org/10.1190/1.3496913>.
- Kennedy, J., Eberhart, R., 1995. Particle swarm optimization. In: *Proceedings of ICNN'95 - International Conference on Neural Networks*. IEEE, Perth, WA, Australia, pp. 1942–1948. <https://doi.org/10.1109/ICNN.1995.488968>.
- Khare, V., Rape, T., 2007. Density inversion using joint PP/PS data: sensitivity to the angle range. In: *77th Annual International Meeting, SEG, Expanded Abstracts*, pp. 965–969. USA.
- Lavaud, B., Kabir, N., Chavent, G., 1999. Pushing AVO inversion beyond linearized approximation. *J. Seismic Explor.* 8 (3), 279–302. <https://doi.org/10.3997/2214-4609.201407876>.
- Li, K., Yin, X., Zong, Z., Lin, H., 2021. Direct estimation of discrete fluid facies and fluid indicators via a Bayesian Seismic Probabilistic Inversion and a novel exact PP-wave reflection coefficient. *J. Petrol. Sci. Eng.* 196, 107412. <https://doi.org/10.1016/j.petrol.2020.107412>.
- Liu, C., Xia, Q., 2004. Offshore multi-wave seismic exploration in Bohai. *Appl. Geophys.* 1, 26–30. <https://doi.org/10.1007/s11770-004-0025-x>.
- Liu, X., Chen, X., Cheng, J., Zhou, L., Chen, L., Li, C., Zu, S., 2023a. Simulation of complex geological architectures based on multistage generative adversarial networks integrating with attention mechanism and spectral normalization. *IEEE Trans. Geosci. Rem. Sens.* 61, 1–15. <https://doi.org/10.1109/TGRS.2023.3294493>.

- Liu, X., Lyu, F., Chen, L., Li, C., Zu, S., Wang, B., 2024. Seismic random noise suppression based on deep image prior and total variation. *IEEE Trans. Geosci. Rem. Sens.* 62, 1–11. <https://doi.org/10.1109/TGRS.2024.3371714>.
- Liu, X., Zhou, H., Guo, K., Li, C., Zu, S., Wu, L., 2023b. Quantitative characterization of shale gas reservoir properties based on Bi-LSTM with attention mechanism. *Geosci. Front.* 14 (4), 101567. <https://doi.org/10.1016/j.gsf.2023.101567>.
- Lu, J., Yang, Z., Wang, Y., Shi, Y., 2015. Joint PP and PS AVA seismic inversion using exact Zoeppritz equations. *Geophysics* 80 (5), R239–R250. <https://doi.org/10.1190/geo2014-0490.1>.
- Meng, J., Zhou, Y.J., Ye, T.R., Xiao, Y.T., Lu, Y.Q., Zheng, A.W., Liang, B., 2023. Hybrid data-driven framework for shale gas production performance analysis via game theory, machine learning, and optimization approaches. *Petrol. Sci.* 20, 277–294. <https://doi.org/10.1016/j.petsci.2022.09.003>.
- Miao, F., He, Y., Wang, S., Huang, H., 2024. A novel fluid identification method based on a high-precision spectral decomposition method. *J. Geophys. Eng.* 21 (2), 534–547. <https://doi.org/10.1093/jge/gxae007>.
- Ostrander, W.J., 1984. Plane-wave reflection coefficients for gas sands at nonnormal angles of incidence. *Geophysics* 49, 1637–1648. <https://doi.org/10.1190/1.1441571>.
- Ouyang, F., Liu, X.Z., Wang, B., Hu, Z.D., Zhao, J.G., Yan, X.Y., Zhang, Y., Qing, Y.H., 2023. The applicability and underlying factors of frequency-dependent amplitude-versus-offset (AVO) inversion. *Petrol. Sci.* 20 (4), 2075–2091. <https://doi.org/10.1016/j.petsci.2023.02.011>.
- Pan, X., Zhang, G., Chen, H., Yin, X., 2017. MCMC-based AVAZ direct inversion for fracture weaknesses. *J. Appl. Geophys.* 138, 50–61. <https://doi.org/10.1016/j.jappgeo.2017.01.015>.
- Pan, X., Zhang, G., Yin, X., 2019. Amplitude variation with offset and azimuth inversion for fluid indicator and fracture weaknesses in an oil-bearing fractured reservoir. *Geophysics* 84 (3), N41–N53. <https://doi.org/10.1190/geo2018-0554.1>.
- Russell, B.H., Hampson, D.P., Hirsche, K., Peron, J., 2005. Joint simultaneous inversion of PP and PS angle gathers. In: *SEG Annual Meeting*, pp. 6–11.
- Shi, J.X., Zhao, X.Y., Zeng, L.B., Zhang, Y.Z., Zhu, Z.P., Dong, S.Q., 2024. Identification of reservoir types in deep carbonates based on mixed-kernel machine learning using geophysical logging data. *Petrol. Sci.* 21 (3), 1632–1648. <https://doi.org/10.1016/j.petsci.2023.12.016>.
- Shuey, R.T., 1985. A simplification of the Zoeppritz equations. *Geophysics* 50 (1), 609–614. <https://doi.org/10.1190/1.1441936>.
- Smith, G.C., Gidlow, P.M., 1987. Weighted stacking for rock property estimation and detection of gas. *Geophys. Prospect.* 35 (9), 993–1014. <https://doi.org/10.1111/j.1365-2478.1987.tb00856.x>.
- Song, B., Li, X.Y., Ding, P., Chen, S., Cai, J., 2023. Direct pre-stack inversion of elastic modulus using the exact Zoeppritz equation and the application in shale reservoir. *Front. Earth Sci.* 11, 1107068. <https://doi.org/10.3389/feart.2023.1107068>.
- Sun, J., Fang, W., Wu, X., Palade, V., Xu, W., 2012. Quantum-Behaved particle swarm optimization: analysis of individual particle behavior and parameter selection. *Evol. Comput.* 20 (3), 349–393. https://doi.org/10.1162/EVCO_a_00049.
- Sun, J., Xu, W., Feng, B., 2004. A global search strategy of quantum-behaved particle swarm optimization. In: *IEEE Conference on Cybernetics and Intelligent System*, pp. 111–116. <https://doi.org/10.1109/ICCIS.2004.1460396>.
- Tang, J., Li, P., Huang, X., Lai, Q., Wang, D., 2023. An exact Zoeppritz based prestack inversion using whale optimization particle filter algorithm under bayesian framework. *IEEE Trans. Geosci. Rem. Sens.* 61, 1–10. <https://doi.org/10.1109/TGRS.2022.3223060>.
- Verma, M., Sreejeth, M., Singh, M., Babu, T.S., Alhelou, H.H., 2022. Chaotic mapping based advanced aquila optimizer with single stage evolutionary algorithm. *IEEE Access* 10, 89153–89169. <https://doi.org/10.1109/ACCESS.2022.3200386>.
- Wang, P.Q., Liu, X.Y., Li, Q.C., Zhou, X.W., Feng, Y.F., 2023. Nonlinear inversion method of russell's fluid factor based on exact-Zoeppritz equation. *IEEE Trans. Geosci. Rem. Sens.* 61, 1–14. <https://doi.org/10.1109/TGRS.2023.3294501>.
- Wang, Y.R., Zong, Z.Y., Yin, X.Y., 2022. Fluid discrimination incorporating amplitude variation with angle inversion and squirt flow of the fluid. *Petrol. Sci.* 19 (4), 1592–1604. <https://doi.org/10.1016/j.petsci.2022.03.007>.
- Yan, F., Han, D.H., Yao, Q., 2021. Rock-physics constrained seismic anisotropy parameter estimation. *Geophysics* 86 (4), MR247–MR253. <https://doi.org/10.1190/geo2019-0153.1>.
- Yang, C., Wang, Y., 2022. Joint PP-PS seismic prestack inversion of thin-bed reservoirs. *J. Geophys. Eng.* 19 (4), 897–913. <https://doi.org/10.1093/jge/gxac060>.
- Yin, X., Zhang, S., 2014. Bayesian inversion for effective pore-fluid bulk modulus based on fluid-matrix decoupled amplitude variation with offset approximation. *Geophysics* 79 (5), R221–R232. <https://doi.org/10.1190/geo2013-0372.1>.
- Zhi, L., Chen, S., Song, B., Li, X., 2018. Nonlinear PP and PS joint inversion based on the exact Zoeppritz equations: a two-stage procedure. *J. Geophys. Eng.* 15 (2), 397–410. <https://doi.org/10.1088/1742-2140/aa9a5c>.
- Zhou, D.Y., Yin, X.Y., Wen, X.T., He, X.L., He, Z.H., 2022. First-order approximate analytical expressions of oblique incident elastic wave at an interface of porous media saturated with a non-viscous fluid. *Petrol. Sci.* 19 (6), 2720–2740. <https://doi.org/10.1016/j.petsci.2022.10.009>.
- Zhou, L., Li, J., Chen, X., Liu, X., Chen, L., 2017. Prestack amplitude versus angle inversion for Young's modulus and Poisson's ratio based on the exact Zoeppritz equations. *Geophys. Prospect.* 65 (6), 1462–1476. <https://doi.org/10.1111/1365-2478.12493>.
- Zhou, L., Li, J., Yuan, C., Liao, J., Chen, X., Liu, Y., Pan, S., 2022. Bayesian deterministic inversion based on the exact reflection coefficients equations of transversely isotropic media with a vertical symmetry axis. *IEEE Trans. Geosci. Rem. Sens.* 60, 1–15. <https://doi.org/10.1109/TGRS.2022.3176628>.
- Zhou, L., Liu, X., Li, J., Liao, J., 2021. Robust AVO inversion for the fluid factor and shear modulus. *Geophysics* 86 (4), R471–R483. <https://doi.org/10.1190/geo2020-0234.1>.
- Zong, Z., Yin, X., Wu, G., 2012. Fluid identification method based on compressional and shear modulus direct inversion. *Chin. J. Geophys.* 55 (1), 284–292. <https://doi.org/10.6038/jj.issn.0001-5733.2012.01.028.2> (in Chinese).